Sensors and Actuators A 259 (2017) 112–120

Contents lists available at ScienceDirect

Sensors and Actuators A: Physical

journal homepage: www.elsevier.com/locate/sna

PVDF based flexible piezoelectric nanogenerators using conjugated polymer:PCBM blend systems

Eui Jin Ko[a], Eui Jin Lee[a], Min Hee Choi[a], Tae Hyun Sung[b], Doo Kyung Moon[a,*]

[a] Department of Materials Chemistry and Engineering, Konkuk University, 1 Hwayang-dong, Gwangjin-gu, Seoul 143-701, Republic of Korea
[b] Department of Electrical Engineering, Hanyang University, 222 Wangsimni-ro, Seongdong-gu, Seoul 136-791, Republic of Korea

ARTICLE INFO

Article history:
Received 7 October 2016
Received in revised form 28 February 2017
Accepted 11 March 2017
Available online 14 March 2017

Keywords:
Conjugated polymer
PCBM
Blend system
PVDF
Piezoelectric nanogenerator

ABSTRACT

Piezoelectric energy harvesting technology has received much attention as a powerful source of energy for a self-powered system. In this study, three main conjugated polymers that have delocalized π-electrons and excellent charge transport properties were studied: poly(3-hexylthiophene) (P1), poly[(4,8-di-(2-ethylhexyloxy)benzo[1,2-b:4,5-b′]dithiophene-2,6-diyl)-alt-(5,5′-yl-4,4′-bis(dodecyl)-2,2′-bithiophene)] (P2) and poly[(4,8-di-(2-ethylhexyloxy)benzo[1,2-b:4,5-b′]dithiophene-2,6-diyl)-alt-(5,5′-yl-4,4′-bis(2-ethylhexyl)-2,2′-bithiophene)] (P3). Each of three polymers was blended with phenyl-C61-butyric acid methyl ester ($PCBM_{61}$), and the blend systems were used to make PVDF based piezoelectric nanogenerators (PNG-0–3). Polymers showed bimodal structures that have a majority edge-on orientation, forming a minority face-on orientation. At a 2 Hz frequency and 0.2 mm displacement, the output voltages (peak-to-peak) of PNG-(0–3) were 35.0 V, 41.2 V, 42.2 V and 43.1 V, respectively, and the output currents (peak-to-peak) were 558.5 nA, 569.5 nA, 572 nA and 589 nA, respectively. The energy conversion efficiencies of PNGs (0–3) were 6.47%, 11.62%, 13.36%, and 14.33%, respectively; therefore, the efficiency was improved by up to about 2.2 times.

1. Introduction

As the market for portable and wearable electronics, such as smartphones, smart watches, tablets, body sensors and medical devices, rapidly grows, electronics based on low-power technologies are playing an increasing role in our everyday lives [1–6]. Accordingly, there have been many studies on self-powered systems using various applications, such as piezoelectric, triboelectric, and electromagnetic energy conversions [7–12].

Some examples of mechanical energy in our daily lives are body motions, vibration, pressure, wind, sound-waves, waterfalls, and so on. This mechanical energy can be converted to electrical energy using a piezoelectric energy harvesting technology, which has been proven to be a powerful source of energy [13–19].

As piezoelectric energy conversion materials, lead zirconate titanate (PZT), barium titanate ($BaTiO_3$), zinc oxide (ZnO) and poly(vinylidene fluoride) (PVDF), have been used in many studies [20–27]. Although piezoelectric properties are one of the most important features, these materials should also be robust against environmental impact, vibration and pressure. In addition, they should meet biocompatibility and environmental considerations.

Organic piezoelectric materials have shown good flexibility and can be used in applications where large deformation is required. Particularly, PVDF is known to be a semicrystalline polymer that has excellent piezoelectric properties. PVDF can have four different crystalline phases: the α, β, γ and δ-phases. The α-phase shows non-polar properties. The β-phase shows polar properties and can be created by mechanical and electrical polling. The excellent piezoelectric properties come from the TTTT (all trans) conformation, where the $-CH_2$ and $-CF_2$ groups of molecular structure are ordered in opposing directions along the polymer main chain [28].

However, since PVDF has relatively lower piezoelectric coefficients (d_{ij}) than ceramic materials, there have been many attempts to increase their output performance [29,30]. Kim et al. proposed a micropatterning of trigonal line-shaped and pyramid-shaped surfaces on P(VDF-TrFE) film-based piezoelectric nanogenerators(PNG). These surfaces yielded higher sensitivity than a flat film [16]. Ou et al. fabricated textile-fiber-based PVDF nonwoven fiber fabric (NFF) harvesters using a hollow cylindrical near-field electrospinning (HCNFES) process to control the diameter, length and density of the fiber [31]. Kim et al. fabricated hybrid-type piezoelectric nanogenerators using both $BaTi_{(1-x)}Zr_xO_3$ nanocubes and PVDF

* Corresponding author.
E-mail address: dkmoon@konkuk.ac.kr (D.K. Moon).

http://dx.doi.org/10.1016/j.sna.2017.03.013
0924-4247/

[32]. J H Yang et al. reported research on the interaction between $-CH_2$ and $-CF_2$ groups of PVDF and functional groups of graphene oxide (GO). Particularly, they presented composites in which PVDF created β-phase crystallites by using graphene oxide [33].

In recent years, there have been many efforts to use conjugated polymers in piezoelectric devices. S W Kim et al. blended poly(3-hexylthiophene) (P3HT) with fullerene derivatives and successfully formed a *p-n* junction with ZnO. In their study, P3HT removed free carriers in ZnO to increase the piezoelectric potential and thus increased the output power [34–36].

Conjugated polymers containing abundant delocalized π-electrons have been used in Organic electronics due to their proper charge transfer property [37]. Benzo[1,2-b:4,5-b′]dithiophene (BDT) is a good candidate for this type of polymer, which has planar and rigid structure having good π-π stacking property. This is beneficial for charge transport. For this reason, polythiophene containing BDT showed high charge mobility [38], and it would help high output power due to more drift charges through external circuit in piezoelectric nanogenerators(PNGs).

In the present study, P3HT (P1) and two types of BDT containing polymers, poly[(4,8-di-(2-ethylhexyloxy)benzo[1,2-b:4,5-b′]dithiophene-2,6-diyl)-alt-(5,5′-yl-4,4′-bis(dodecyl)-2,2′-bithiophene)] (P2) and poly[(4,8-di-(2-ethylhexyloxy)benzo[1,2-b:4,5-b′]dithiophene-2,6-diyl)-alt-(5,5′-yl-4,4′-bis(2-ethylhexyl)-2,2′-bithiophene)] (P3), were used as electron-rich units. Also, phenyl-C61-butyric acid methyl ester ($PCBM_{61}$), a fullerene derivative, was used as an electron deficient unit. They were mixed together to make blend systems, and introduced to PVDF-based PNGs for increasing output performance.

A control system with no blend was used in PNG-0. The output voltage (OV) (peak-to-peak) and output current (OC) (peak-to-peak) of PNG-0 were 35.0 V and 558.5 nA, respectively. On the other hand, when blend systems of polymers and $PCBM_{61}$ were used in the PNGs-(1–3), their OVs were increased to 41.2 V, 42.2 V, and 43.1 V and their OCs to 569.5 nA, 572 nA, and 589 nA, respectively. The energy conversion efficiencies were 6.47%, 11.62%, 13.36%, and 14.33% for PNG-0, 1, 2, and 3, respectively. As a result, the output power of PNG-(1–3) were increased by up to about 2.2 times compared to PNG-0 by using conjugated polymer blend systems.

2. Experiments

2.1. Materials

All starting materials were purchased from Sigma Aldrich, Alfa Aesar and Tokyo Chemical Industry Co., LTD. and used without an extra purification step. 3-dodecylthiophene was purchased from Sigma Aldrich, 80-μm thick PVDF film from Fils Co. LTD., and P3HT (P1) and $PCBM_{61}$ from One material, Inc. Two types of bithiophene with dodecyl group (2) and 2-ethylhexyl group (5) in scheme S1 and 2,6-bis(trimethyltin)-4,8-bis(2-ethylhexyloxy)benzo[1,2-b:4,5-b′]-dithiophene (a) and the polymers (P2 and P3) in scheme S2 were synthesized according to the Ref. [39].

2.2. Device fabrication and characterization

The fabrication process of the flexible PNG is shown in Fig. S1. PVDF film ($35 \times 35\ mm^2$) was first sonicated with a detergent solution and DI water for cleaning. Then, the film was dried in an oven at 60 °C for 10 min and cleaned with ultraviolet ozone (UVO) cleaner (AH 1700, Ahtech LTS).

P1 and $PCBM_{61}$ were mixed at a ratio of 1:0.6(w/w). This mixture was then blended at a concentration of 42 mg/ml with 1,2-dichlorobenzene(ODCB) to make the solution. The same amounts of P2 and P3 were mixed and blended at a concentration of 21 mg/ml with ODCB to make the solution. These solutions were then spin-coated on the top surface of the pretreated PVDF film at 1000 rpm for 30 s and annealed at 80 °C for 10 min.

On this spin-coated layer, MoO_3 (10 nm) and Ag (100 nm) were thermally evaporated in a high vacuum chamber ($<10^{-7}$ Torr) in sequence. On the bottom side of the PVDF film, Al (100 nm) was thermally evaporated. Finally, the entire film was cut to $25 \times 15\ mm^2$.

2.3. Measurements

The ^1H NMR (400 MHz) spectra of P2 and P3 were measured using a NMR measurement (Bruker AMX400 spectrometer). The thickness of each blend layer (P1–P3:$PCBM_{61}$) was measured using a focused ion beam (Helios nanolab 600, FEI company). A home-made test apparatus was designed and implemented to measure the outputs by repeatedly stretching and releasing the devices at different frequencies (Hz) and displacements (mm). The OVs and OCs were measured using MDO4104C Oscilloscope (Tektronix) with 100MΩ impedance probe (P6015A) and DMM7510 (7.5 digit graphical sampling multimeter, Keithley), respectively.

One side of the fabricated devices was fixed on the test apparatus. The displacement and frequency were set to 0.2 mm and 2 Hz, respectively, and the devices were repeatedly stretched and released.

To examine the crystalline phase of P1-P3 as pristine polymers and the blend systems with $PCBM_{61}$, the solutions, with the same concentration of materials as used in the fabricated devices, were drop-casted on a Si wafer and annealed at 80 °C to make a thin film. The X-ray diffraction (new D8-Advance, Bruker-AXS) patterns of this thin film were measured.

To determine the change of the work function of Ag and Ag with MoO_3 electrodes, ultraviolet photoelectron spectroscopy (UPS) spectra of them were measured using a UPS analysis chamber at 2×10^{-8} Torr with an AXIS Ultra DLD hemispherical electron energy analyzer (KRATOS, Inc.) with He I ($h\nu = 21.2$ eV) source.

Furthermore, to examine the charge-carrier mobility properties of the P1-P3 blend systems, the hole mobility was measured using the space-charge limited current (SCLC) method and calculated using the following equation: $J = \frac{9}{8}\varepsilon\varepsilon_0\mu\frac{V^2}{L^3}\exp\left[0.89\gamma\sqrt{\frac{V}{L}}\right]$, where ε is a dielectric constant, ε_0 is the permittivity of the free space, μ is the mobility, V is a bias voltage, and L is the film thickness [40].

3. Results and discussion

Fig. 1(a–c) shows the structures of the polymers (P1–P3) that were used in the PNG. In addition, Fig. 1(d) shows the structure of the β-phase PVDF, which has all of the dipoles lined up in the same direction. The yields of P2 and P3 were 80.9% and 87.8%, respectively. This synthesis process is shown in Scheme S2. P2 and P3 are black and red powders, respectively, and they dissolved well in organic solvents, such as chloroform, chlorobenzene, ODCB, THF and toluene. These structures were confirmed using ^1H NMR, as shown in Fig. S2 (a & b). The molecular weights for P1 were 35.4 kDa (Mn) and 78.0 kDa (Mw). Those of P2 were 24.1 kDa (Mn) and 53.2 kDa (Mw). Those of P3 were 28.3 kDa (Mn) and 52.8 kDa (Mw). Furthermore, the polydispersity index (PDI) for P1–P3 were 2.20, 2.21 and 1.87, respectively, indicating a relatively narrow distribution. These values are summarized in Table S1.

Fig. 2 shows the PNG structure (a and b, $25 \times 15\ mm^2$) and the cross-sectional SEM images of the top side of PNGs (c–e). All of the Ag electrodes of samples were deposited by Pt layer to protect the damage of Ag surface from Ga ion source during milling

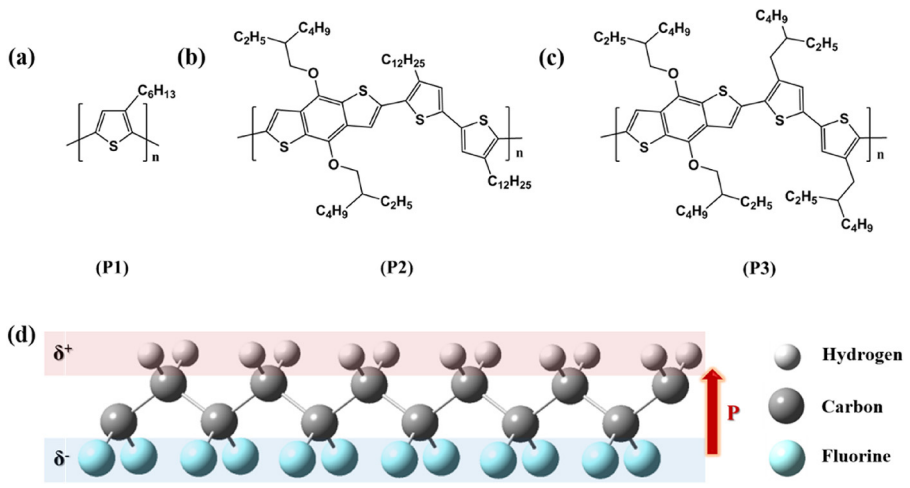

Fig. 1. Conjugated polymers ((a) P1, (b) P2 and (c) P3) and (d) the structure of β-phase PVDF.

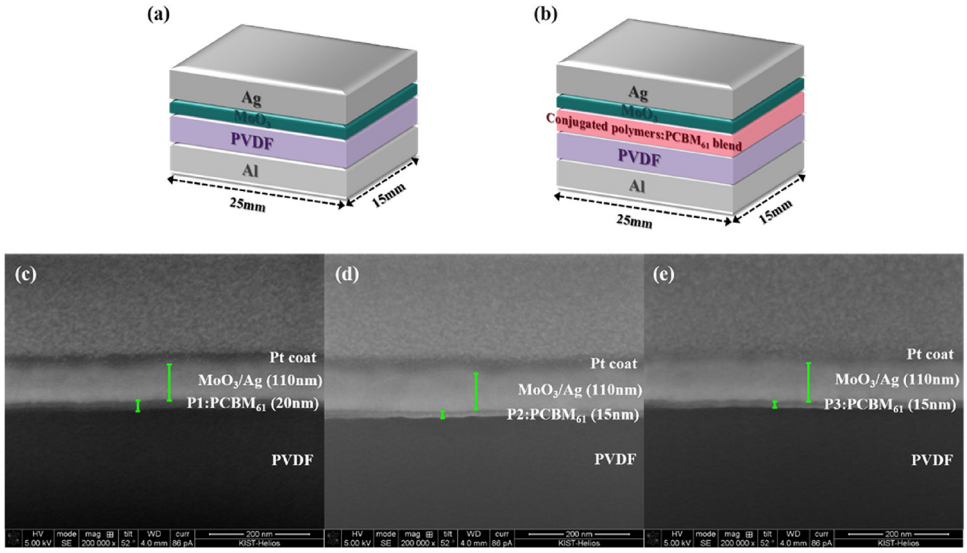

Fig. 2. The PNG; (a) without conjugated polymer:$PCBM_{61}$ blend system(PNG-0), (b) with conjugated polymer:$PCBM_{61}$ blend systems (PNG-(1 3)). All the devices are $25 \times 15\ mm^2$. Cross-sectional SEM images of the PNGs using focused ion beam(FIB); (c) PNG-1, (d) PNG-2 and (e) PNG-3. Pt was deposited on Ag electrodes to protect the damage from Ga ion source during milling process.

process and to get images with accurate thickness of layer by layer. Fig. 2(a) shows the PNG-0 structure (Al/PVDF/MoO_3/Ag), and Fig. 2(b) shows the PNG-(1–3) structures (Al/PVDF/blend layer (P1–P3:$PCBM_{61}$)/MoO_3/Ag). The cross-sectional SEM images in Fig. 2(c–e) show the top side of PNG-(1–3) where the blend layers were introduced. It was observed that the thicknesses of the blend layers in (c)–(e) were 20 nm, 15 nm, and 15 nm, respectively.

3.1. Piezoelectric properties

Fig. 3(a) shows a measurement image of the home-made test apparatus that was designed and implemented to measure the piezoelectric properties of the PNGs-(0–3). In Fig. 3(a), one side of the device in the dashed circle was fixed at the test apparatus, and the other side was repeatedly stretched and released by 0.2 mm. As shown in Fig. 3(b), the top and bottom electrodes were connected to the oscilloscope and the multimeter to measure OVs and OCs, respectively. The outputs were measured when the device was stretched and released, and the measured schematic diagram of the device is shown in Fig. 3(c) and (d). When there is no strain on the device, the output was 0, as shown in Fig. 3(b). All of the dipoles in β-phase PVDF were lined up in the same direction, as shown in Fig. 1(d). When a stretching force is applied along the uniaxial direction, as shown in Fig. 3(c), the dipole moment increases due to the piezoelectric effect, and the total spontaneous polarization increases as well. As a result, the positive and negative piezoelectric potentials of the PVDF film increase ($V^+ \rightarrow V^{++}, V^- \rightarrow V^{--}$), and this in turn generates a positive pulse. As shown in Fig. 3(d), a negative pulse is generated when the device is released. The positive piezoelectric potential (V^+) generates repulsive and attractive forces to the hole (h^+) and electron (e^-), respectively, and the negative piezoelectric potential (V^-) generates forces in reverse.

When the strain force is applied, the piezoelectric potential of the PVDF drives carriers from one electrode to the other through the external circuit. As shown in Fig. 3(c), when the device is stretched, the delocalized π-electrons (e^-) in the conjugated polymers in the blend systems move to the positive piezoelectric potential (V^{++}) of the PVDF through electron acceptors ($PCBM_{61}$) and become trapped. Holes (h^+) flow from the top electrode to the bottom electrode [41,42].

This mechanism is similar to the work by S W Kim et al. in that the piezoelectric potential was increased by using ZnO as a

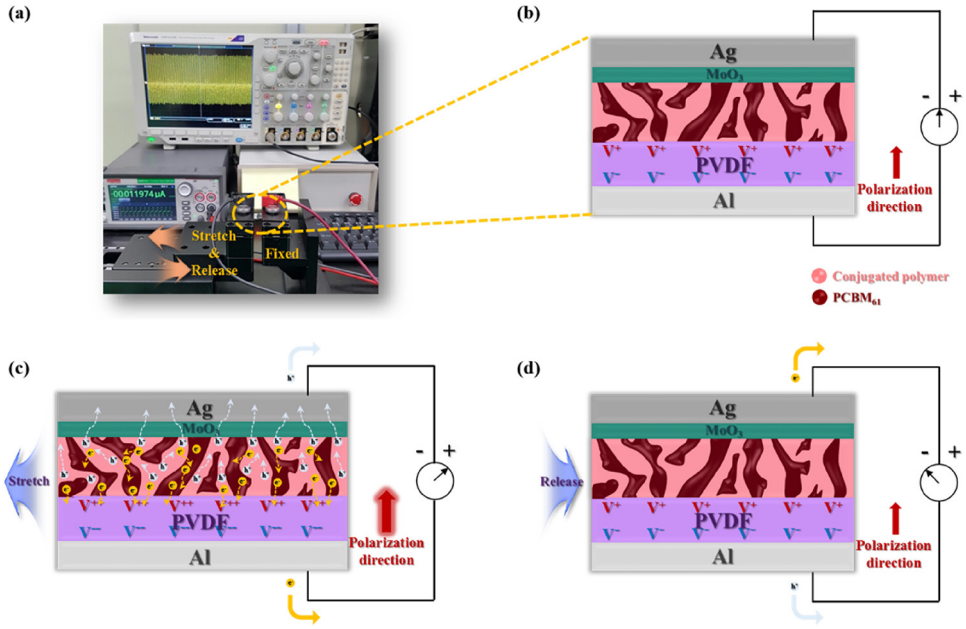

Fig. 3. Schematic descriptions of the PNGs using conjugated polymer:$PCBM_{61}$ blend systems; (a) the image of a PNG tested by the home-made tester, (b) schematic illustration of the PNG with no strain, (c) diagram of the PNG after applied strain and (d) release.

Table 1
The average of measured output voltages & currents (peak-to-peak) of piezoelectric nanogenerators.

	Voltage [V]	Current [nA]
PNG-0	35.0	558.5
PNG-1	41.2	569.5
PNG-2	42.2	572
PNG-3	43.1	589

piezoelectric material and forming a *p-n* junction with the ZnO and P3HT:PCBM layer. More specifically, P3HT:PCBM led to a large enhancement in the output voltage due to the passivation of free electrons in ZnO and decreased the total capacitance and increased the Fermi level difference between the two electrodes. Furthermore, they used graphene as electrodes and modified the mobility according to the polarization direction of P(VDF-TrFE), and this new type of stretchable nanogenerator was fabricated on a PDMS substrate [34,41].

We made several PNGs with different structures to fabricate an optimal structure for PNG with blend systems. As shown in Fig. S3, the PNG with same electrodes on both sides showed low outputs in the case of Al or Ag (~25 V). However, a PNG with different electrodes on each side showed higher performance than the one with same electrodes (~39 V). Also, when a high work function material, molybdenum trioxide (MoO_3), was introduced as a hole transport layer between blend layers and top electrodes to extract holes efficiently from P1–P3, the output performance was more increased compared to same electrodes (25 V → 32 V) (Fig. S3(b)&(d)). Therefore, we chose the optimized structure which is Al/PVDF/blend layers/MoO_3/Ag.

Fig. 4 shows the OVs (a–d) and OCs (e–h) of all of the PNGs that were measured in the test shown in Fig. 3(a). Each device was repeatedly stretched and released for 20 s at a 2 Hz frequency and 0.2 mm displacement. The averaged OV (peak-to-peak: V) and OC (peak-to-peak: nA) of PNG-0 (a & e: black line) were 35.0 V and 558.5 nA, respectively. (+) pulse and (−) pulse were observed in PNG-1 (b & f: red line), PNG-2 (c & g: blue line) and PNG-3 (d & h: green line) as in PNG-0. The OV and OC results of each PNG are summarized in Table 1. The OVs of PNG-(1–3) were 41.2 V, 42.2 V, and 43.1 V, respectively, and the OCs of PNG-(1–3) were 569.5 nA, 572 nA, and 589 nA, respectively.

To calculate d_{32} constants, we used the following equation:

$$d_{32} = \frac{\varepsilon_0 \varepsilon_r V}{t\sigma}$$

where ε_0 is the dielectric constant of the air (8.85×10^{-12} F/m), ε_r is the relative dielectric constant of PVDF (13 ± 1), V is the voltage, t is the thickness and σ is stress. σ was calculated by $\sigma = E \cdot \varepsilon$, where E is Young's modulus (3 GPa) and ε is strain ($\Delta L/L = 0.008$) [43]. The calculated d_{32} of PVDF untreated/treated by blend systems in PNG-(0–3) are 2.10 pC/N, 2.47 pC/N, 2.53 pC/N and 2.58 pC/N, respectively. For g_{32} constants, the values of PVDF in PNG-(0–3) were calculated using $g_{32} = \frac{d_{32}}{\varepsilon_0 \varepsilon_r}$, which are 1.82×10^{-2} Vm/N, 2.15×10^{-2} Vm/N, 2.20×10^{-2} Vm/N and 2.24×10^{-2} Vm/N, respectively. d_{32} and g_{32} of the original β-phase PVDF film were given by Fils Co. Ltd., which are 2.00 pC/N and 2.0×10^{-2} Vm/N, respectively. The values of PVDF without blend system (PNG-0) were almost same as above. However, the values of PVDF with blend systems (PNG-(1–3)) were slightly improved depending on the increased voltages by up to 29% in the case of d_{32} and 12% in the case of g_{32}.

The energy conversion efficiency (η) of the fabricated piezoelectric nanogenerators were calculated by dividing the electrical energy (W_e) by the mechanical energy (W_m) as in the following equation:

$$\eta = \frac{W_e}{W_m} \times 100\,(\%)$$

As shown in Fig. S4, a stress-strain curve was measured by an UTM instrument, and the mechanical energy (W_m) was calculated by integrating stress with displacement from 0 mm (initial) to 0.2 mm (final) using $W_m = \int_{F_i}^{F_f} F_x dx$. The W_m was 6.48×10^{-5} J. Also, the electrical energy was calculated using $W_e = \int \frac{V^2}{R} dt$, and integrated for one cycle. The calculated electrical energies (W_e) for

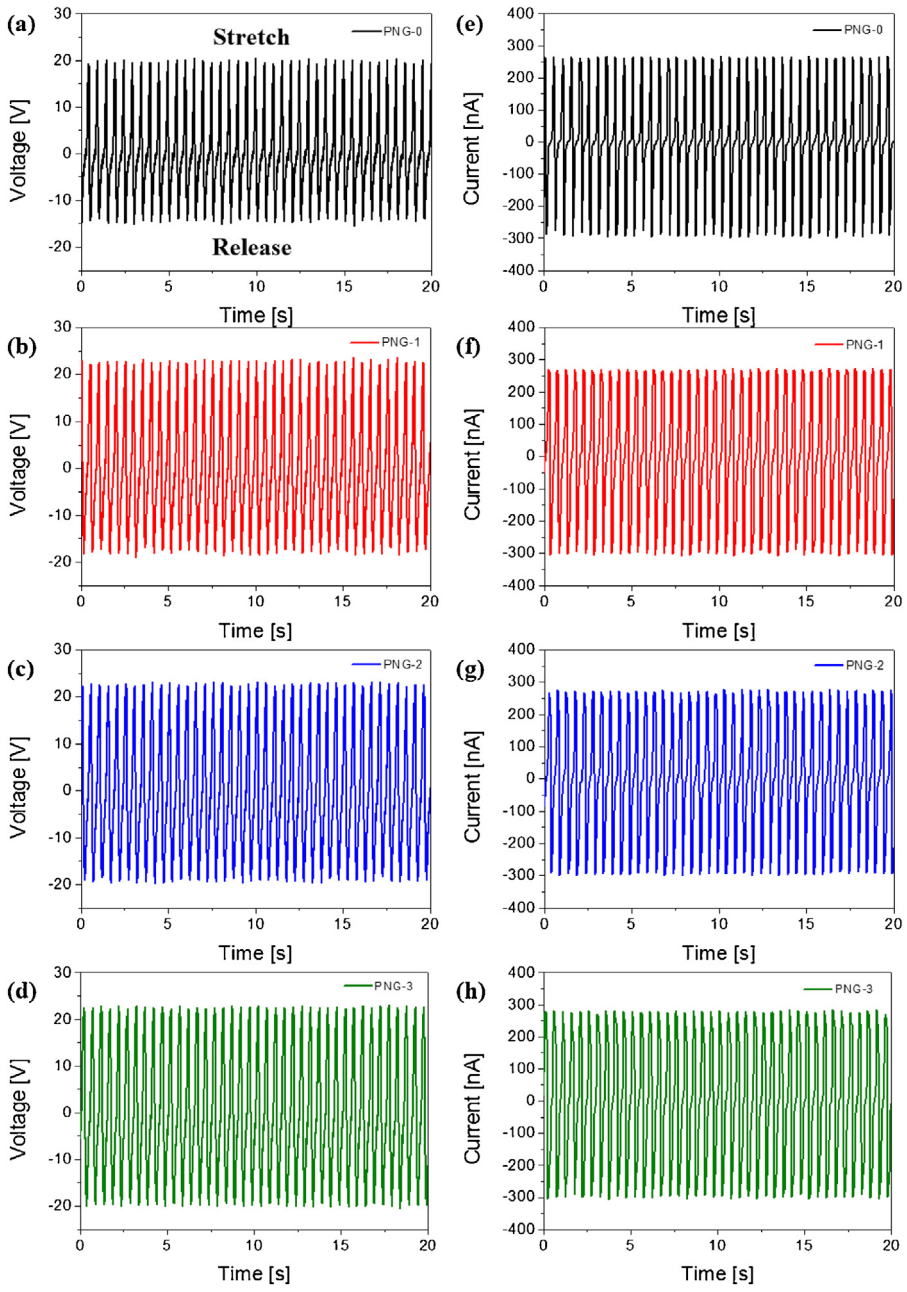

Fig. 4. The OVs (a–d) and OCs (e–h) of PNGs at 2 Hz; PNG-0 (a, e; black line), PNG-1 (b, f; red line), PNG-2 (c, g; blue line) and PNG-3 (d, h; green line). (For interpretation of the references to color in this figure legend, the reader is referred to the web version of this article.)

the PNGs-(0–3) were 4.19×10^{-6} J, 7.53×10^{-6} J, 8.66×10^{-6} J and 9.29×10^{-6} J, respectively.

The calculated energy conversion efficiency (η) results were 6.47%, 11.62%, 13.36%, and 14.33% for PNG-(0–3), respectively. These results suggest that the conjugated polymer blend system helps to improve the efficiency. Moreover, it has been shown that P2 and P3 have better performance than P1 due to the BDT unit, which has a better planarity and charge transfer property than the thiophene in P1. P3 had a better performance than P2 due to the superior alkyl chain in P3 (linear alkyl chain in P2 and branched alkyl chain in P3).

3.2. X-ray diffraction properties

In Fig. 5, the XRD patterns of the pristine polymers (P1–P3) and blend layers (P1–P3:$PCBM_{61}$ = 1:0.6(w/w)) are shown. Fig. 5(a) shows the XRD patterns of the pristine polymer films in out-of-plane mode. The diffraction peaks were very sharp and clear at $2\Theta = 5.41$, 4.05, and 5.49°. This is a lamellar structure (100) that forms an edge-on orientation perpendicular to the substrates. The lamellar d-spacing distance (d_1) between molecules was calculated using Bragg's law ($\lambda = 2d\sin\Theta$) and determined to be 16.32, 21.79, and 16.08 Å. P2 showed the longest distance among the three. This is because the linear dodecyl side chain consists of more carbons than the hexyl group in P1 (6 carbons) and the branched 2-ethylhexyl in P3 (8 carbons). Fig. 5(b) shows the XRD patterns of the pristine polymer films in in-plane mode. Diffraction peaks were observed at $2\Theta = 5.08$, 3.74, and 5.39°, and these results verify that P1–P3 are all bimodal structures that have a majority edge-on orientation, forming a minority face-on orientation[44].

In Fig. 5(c), the XRD pattern of the blend film with a ratio of polymers and $PCBM_{61}$ of 1:0.6(w/w) is shown. The (100) peak of

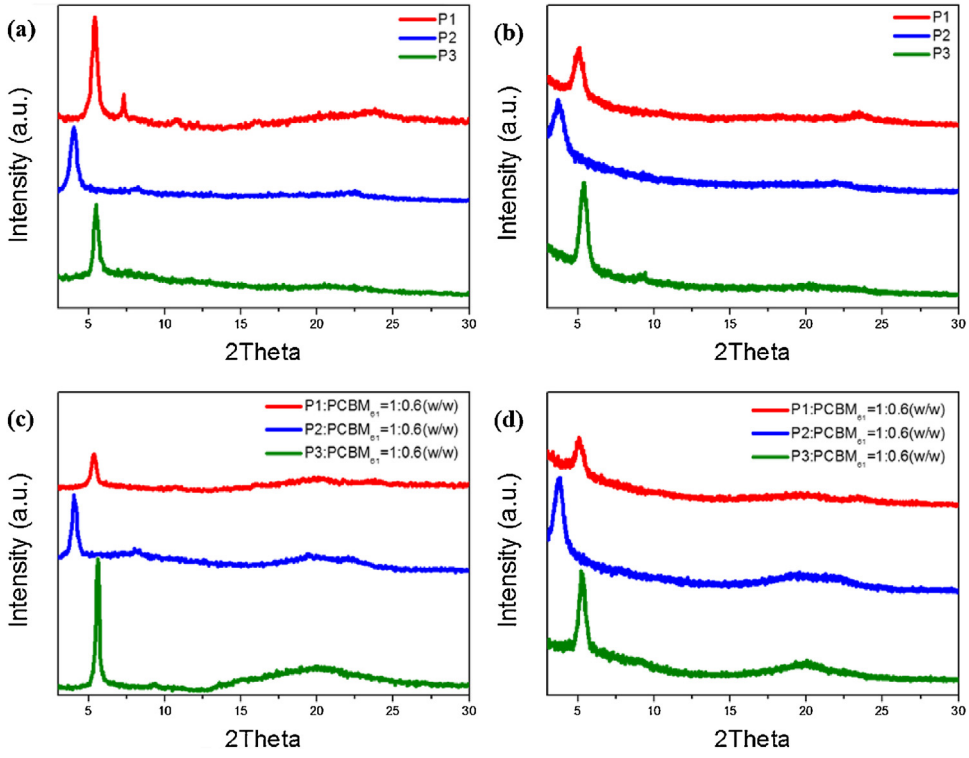

Fig. 5. X-ray diffraction patterns of pristine polymers (P1–P3) and blended films (P1–P3):$PCBM_{61}$ = 1:0.6(w/w); (a & c) out-of-plane mode, (b & d) in-plane mode.

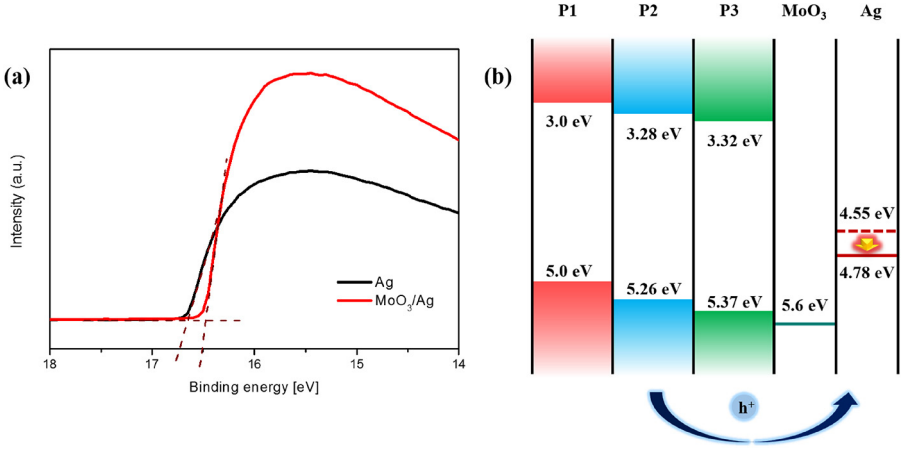

Fig. 6. UPS spectra of Ag and MoO3/Ag (a) and energy band diagram of P1 P3/MoO_3/Ag.

P1 was observed at 2Θ = 5.37°, and the lamellar d-spacing distance (d_1) slightly increased from 16.32 Å (pristine polymer) to 16.44 Å. P2 had a (100) peak at 2Θ = 4.05°, and d_1 was 21.79 Å, which is the same distance as that of the pristine polymer. P3 had a (100) peak at 2Θ = 5.61°, and d_1 was slightly decreased from 16.08 Å (pristine polymer) to 15.73 Å. Fig. 5(d) shows the XRD pattern of the blend film in in-plane mode, and the pattern is similar to that of the pristine polymer. It was also observed that all of the polymers form a majority edge-on orientation and minority face-on orientation.

3.3. Ultraviolet photoelectron spectroscopy

In Fig. 6(a), we measured UPS spectra of Ag and Ag with MoO_3. The work function of Ag was 4.55 eV and Ag with MoO_3 was 4.78 eV, which the work function of Ag was down-shifted with MoO_3 about 0.23 eV compared to the one of Ag only. These value was obtained by $WF = h\nu - E_{cut\text{-}off}$, where $h\nu$ is 21.2 eV (He I). According to the results, energy band diagram of polymers (P1–P1)/MoO_3/Ag was depicted in Fig. 6(b). The energy level barrier between polymers (P1–P3) and Ag was decreased by the introduction of MoO_3, which is a good hole extraction material[45]. Therefore, holes from polymers could flow to Ag electrode easily. The HOMO levels of P1–P3 were 5.0, 5.26 and 5.37 eV [39]. Especially in the case of P3, the HOMO level is similar to the work function of MoO_3 (5.6 eV), which is like ohmic contact. Therefore, when force inputs to PNGs, more charges can flow through the external circuits to get high output performance.

3.4. Charge carrier mobility properties

Hole-only devices were fabricated, and the sequence of the fabricated layers were as follows: ITO/PEDOT:PSS/(P1–P3):$PCBM_{61}$ = 1:0.6(w/w)/MoO_3/Ag. The hole mobility measurement results are shown in Fig. 7. The measured hole mobilities were 1.52×10^{-6} $cm^2/V\,s$, 1.84×10^{-6} $cm^2/V\,s$, and

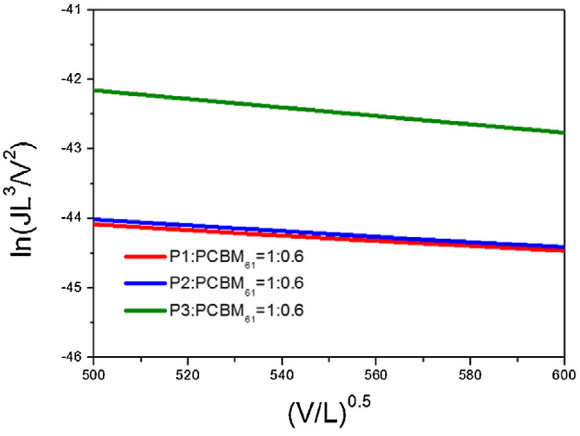

Fig. 7. J-V characteristics of conjugated polymers (P1–P3):$PCBM_{61}$ = 1:0.6(w/w); hole-only device. (ITO/PEDOT:PSS/conjugated polymers:$PCBM_{61}$ = 1:0.6(w/w)/MoO_3/Ag).

Table 2
Film thickness and hole mobilities of conjugated polymers:$PCBM_{61}$ = 1:0.6(w/w).

Polymer:$PCBM_{61}$ = 1:0.6 (w/w)	Film thickness [nm]	Hole mobility [cm^2/V s]
P1	20	1.52×10^{-6}
P2	15	1.84×10^{-6}
P3	15	3.64×10^{-5}

3.64×10^{-5} cm^2/V s for the P1–P3 blend systems, respectively. The hole mobility measurements are summarized in Table 2.

P1 consists of thiophene only, while the BDT moiety was introduced in P2 and P3. This difference makes P2 and P3 have a better performance. PNG-2 with P2 has a higher performance than PNG-1 with P1 about 15%, while PNG-3 with P3 is better than the one with P1 about 23%.

As the hole mobility of the conjugated polymer increased, the output performance of the PNG improved. This is because more charge flowed from the blend layer to the lower electrode through the external circuit and in reverse.

3.5. Morphology properties

Fig. 8 shows the topographies (a–c) and phase images (d–f) of (P1–P3):$PCBM_{61}$ blend films formed on the PVDF film. In case of the P1 blend (Fig. 8(a) & (d)), a large domain was formed, which led to a poor network between the polymer and $PCBM_{61}$ and a large RMS roughness of 9.488 nm. Although the P2 blend (Fig. 8(b) & (e)) has polymer-only domains, such as islands, the network between the polymer and $PCBM_{61}$ was relatively smoother than that of P1. The RMS roughness was 1.238 nm and showed a smooth morphology. The P3 blend (Fig. 8(c) & (f)) formed 10–30 nm polymer-only domains and 10–30 nm $PCBM_{61}$ clusters. It was observed that the P3 blend had the finest channel among the three polymers. The RMS roughness was 1.290 nm and showed a very smooth and overall intermixed network. Due to this better charge pathway, charges could efficiently move from the blend via the external circuit, and thus, the output performance was improved.

4. Conclusions

In this study, PNGs were fabricated by introducing a blend layer {1:0.6(w/w)} of conjugated polymers (P1–P3) and $PCBM_{61}$ to the top of a β-phase PVDF. It was shown that the polymers of the blend layer are bimodal structures with a majority having an edge-on orientation and minority having a face-on orientation to the substrate. P3, containing thiophene with a branched side chain, showed a higher hole mobility by an order of magnitude. Furthermore, it formed the finest interpenetrating network with $PCBM_{61}$. When a strain force was applied at a 2 Hz frequency and 0.2 mm displacement, the OVs (peak-to-peak) and the OCs (peak-to-peak) were improved when the blend systems were introduced. The d_{32} values of PNG-(0–3) were 2.10 pC/N, 2.47 pC/N, 2.53 pC/N and 2.58 pC/N, respectively. Also, the g_{32} values of them were 1.82×10^{-2} Vm/N, 2.15×10^{-2} Vm/N, 2.20×10^{-2} Vm/N and 2.24×10^{-2} Vm/N, respectively. The energy conversion efficiencies were 6.47%, 11.62%, 13.36%, and 14.33% for PNG-0–3, respectively. This indicates that the efficiencies of PNGs with blend systems were improved by up to 2.2 times over that of PNG-0.

By introducing blend systems consisting of conjugated polymers and $PCBM_{61}$ in the conventional PVDF-based PNGs, the piezoelec-

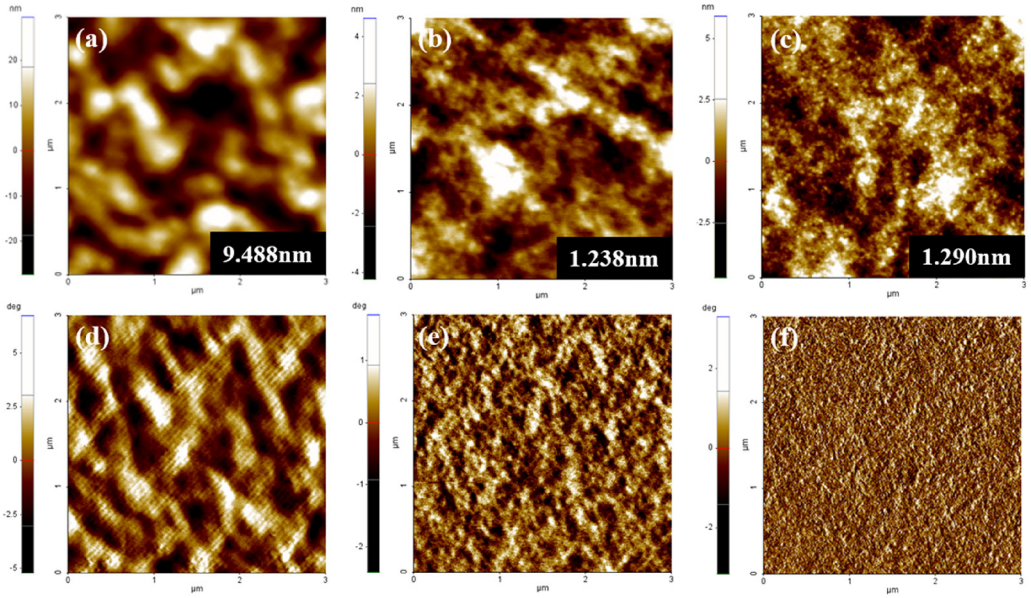

Fig. 8. AFM topography images (a-c) and phase images (d-f) of P1:$PCBM_{61}$ = 1:0.6(w/w) (a and d), P2:$PCBM_{61}$ = 1:0.6(w/w) (b and e) and P3:$PCBM_{61}$ = 1:0.6(w/w) (c and f) (All the images are 3 × 3 μm^2).

tric constants (d & g) were increased, and the output performance was improved due to more drift charges. Therefore, it is expected that the use of blend systems in piezoelectric devices would accelerate the development of the flexible self-powered electronics.

Acknowledgements

This work was supported by the *Energy Efficiency & Resources Core Technology Program of the Korea Institute of Energy Technology Evaluation and Planning (KETEP), granted financial resource from the Ministry of Trade, Industry & Energy, Republic of Korea. (No. 20142020103970)

Appendix A. Supplementary data

Supplementary data associated with this article can be found, in the online version, at http://dx.doi.org/10.1016/j.sna.2017.03.013.

References

[1] Z.L. Wang, W. Wu, Nanotechnology-enabled energy harvesting for self-powered micro-/nanosystems, Angew. Chem. Int. Ed. 51 (2012) 11700–11721.
[2] J. Zhong, Y. Zhang, Q. Zhong, Q. Hu, B. Hu, Z.L. Wang, J. Zhou, Fiber-based generator for wearable electronics and mobile medication, ACS Nano 8 (2014) 6273–6280.
[3] W. Zeng, L. Shu, Q. Li, S. Chen, F. Wang, X.M. Tao, Fiber-based wearable electronics: a review of materials, fabrication, devices, and applications, Adv. Mater. 26 (2014) 5310–5336.
[4] D.J. Lipomi, M. Vosgueritchian, B.C.-K. Tee, S.L. Hellstrom, J. a Lee, C.H. Fox, Z. Bao, Skin-like pressure and strain sensors based on transparent elastic films of carbon nanotubes, Nat. Nanotechnol. 6 (2011) 788–792.
[5] Z. Li, X. Zhang, G. Li, In situ ZnO nanowire growth to promote the PVDF piezo phase and the ZnO-PVDF hybrid self-rectified nanogenerator as a touch sensor, Phys. Chem. Chem. Phys. 16 (2014) 5475–5479.
[6] W. Al-ashtari, M. Hunstig, T. Hemsel, W. Sextro, Enhanced energy harvesting using multiple piezoelectric elements: theory and experiments, Sens. Actuators A Phys. 200 (2013) 138–146.
[7] W.S. Jung, M.J. Lee, M.G. Kang, H.G. Moon, S.J. Yoon, S.H. Baek, C.Y. Kang, Powerful curved piezoelectric generator for wearable applications, Nano Energy 13 (2015) 174–181.
[8] B.U. Hwang, J.H. Lee, T.Q. Trung, E. Roh, D. Il Kim, S.W. Kim, N.E. Lee, Transparent stretchable self-powered patchable sensor platform with ultrasensitive recognition of human activities, ACS Nano 9 (2015) 8801–8810.
[9] L. Luo, D. Bao, W. Yu, Z. Zhang, T. Ren, A low input current and wide conversion ratio buck regulator with 75% efficiency for high-voltage triboelectric nanogenerators, Sci. Rep. (2016) 1–8.
[10] X. Cheng, B. Meng, X. Chen, M. Han, H. Chen, Z. Su, M. Shi, H. Zhang, Single-Step fluorocarbon plasma treatment-induced wrinkle structure for high-performance triboelectric nanogenerator, Small 12 (2016) 229–236.
[11] Y.H. Ko, G. Nagaraju, S.H. Lee, J.S. Yu, PDMS-based triboelectric and transparent nanogenerators with ZnO nanorod arrays, ACS Appl. Mater. Interfaces 6 (2014) 6631–6637.
[12] B.L. Ooi, J.M. Gilbert, A.R.A. Aziz, Switching damping for a frequency-tunable electromagnetic energy harvester, Sens. Actuators A Phys. 234 (2015) 311–320.
[13] Y. Ivry, N. Wang, C. Durkan, domain engineering High-frequency programmable acoustic wave device realized through ferroelectric domain engineering, Appl. Phys. Lett. 104 (2014) 133505.
[14] M. Kim, J. Dugundji, B.L. Wardle, T. Kajihara, Y. Ueno, Y. Tsujiura, Y. Koshiba, Piezoelectric vibration energy harvesters with stretched and multistacked organic ferroelectric films sensors Piezoelectric vibration energy harvesters with stretched and multistacked organic ferroelectric films, Jpn. J. Appl. Phys. 56 (2017), 04CL04.
[15] K.Y. Lee, D. Kim, J.H. Lee, T.Y. Kim, M.K. Gupta, S.W. Kim, Unidirectional high-power generation via stress-induced dipole alignment from ZnSnO3 nanocubes/polymer hybrid piezoelectric nanogenerator, Adv. Funct. Mater. 24 (2014) 37–43.
[16] J.H. Lee, H.J. Yoon, T.Y. Kim, M.K. Gupta, J.H. Lee, W. Seung, H. Ryu, S.W. Kim, Micropatterned P(VDF-TrFE) film-based piezoelectric nanogenerators for highly sensitive self-powered pressure sensors, Adv. Funct. Mater. 25 (2015) 3203–3209.
[17] S. Siddiqui, D. Il Kim, L.T. Duy, M.T. Nguyen, S. Muhammad, W.S. Yoon, N.E. Lee, High-performance flexible lead-free nanocomposite piezoelectric nanogenerator for biomechanical energy harvesting and storage, Nano Energy 15 (2015) 177–185.
[18] M.J. Johnson, D.B. Go, Piezoelectric transformers for low-voltage generation of gas discharges and ionic winds in atmospheric air, J. Appl. Phys. 118 (2015) 243304.
[19] J. Zhao, J. Yang, Z. Lin, N. Zhao, J. Liu, Y. Wen, P. Li, An arc-shaped piezoelectric generator for multi-directional wind energy harvesting, Sensor Actuat. A: Phys. 236 (2015) 173–179.
[20] P. Janphuang, R. Lockhart, N. Uffer, D. Briand, N.F. De Rooij, Vibrational piezoelectric energy harvesters based on thinned bulk PZT sheets fabricated at the wafer level, Sensor Actuat. A: Phys. 210 (2014) 1–9.
[21] D. Balma, A. Mazzalai, N. Chidambaram, C.S. Sandu, A. Neels, A. Dommann, P. Hess, D. Binz, P. Muralt, High piezoelectric longitudinal coefficients in sol-gel PZT thin film multilayers, J. Am. Ceram. Soc. 97 (2014) 2069–2075.
[22] D.M. Marincel, S. Jesse, A. Belianinov, M.B. Okatan, S.V. Kalinin, T.N. Jackson, C.A. Randall, S. Trolier-McKinstry, A-site stoichiometry and piezoelectric response in thin film $PbZr_{1-x}Ti_xO_3$, J. Appl. Phys. 117 (2015), 204104.
[23] J. Glaum, M. Zakhozheva, M. Acosta, E. Aksel, H. Kleebe, M. Hoffman, L.A. Schmitt, Influence of B-site disorder on the properties of unpoled $Bi_{1/2}Na_{1/2}TiO_3$-0.06$Ba(Zr_xTi_{1-x})O_3$ piezoceramics, J. Am. Ceram. Soc. 99 (2016) 2801–2808.
[24] D. Maurya, Y. Zhou, Y. Yan, S. Priya, Synthesis mechanism of grain-oriented lead-free piezoelectric $Na_{0.5}Bi_{0.5}TiO_3$-$BaTiO_3$ ceramics with giant piezoelectric response, J. Mater. Chem. C 1 (2013) 2102–2111.
[25] N. Jalali, J. Briscoe, P. Woolliams, M. Stewart, P. Weaver, M. Cain, S. Dunn, Passivation of zinc oxide nanowires for improved piezoelectric energy harvesting devices, J. Phys.: Conf. Ser. 476 (2013) 012131.
[26] N. Soin, D. Boyer, K. Prashanthi, S. Sharma, A.A. Narasimulu, J. Luo, T.H. Shah, E. Siores, T. Thundat, Exclusive self-aligned β-phase PVDF films with abnormal piezoelectric coefficient prepared via phase inversion, Chem. Commun. 51 (2015) 8257–8260.
[27] V. Bhavanasi, D.Y. Kusuma, P.S. Lee, Polarization orientation piezoelectricity, and energy harvesting performance of ferroelectric PVDF-TrFE nanotubes synthesized by nanoconfinement, Adv. Energy Mater. 4 (2014) 1–8.
[28] V. Sencadas, R. Gregorio, S. Lanceros-Mendez, α to β phase transformation and microestructural changes of PVDF films induced by uniaxial stretch, J. Macromol. Sci. Part B 48 (2009) 514–525.
[29] C.R. Bowen, H. a. Kim, P.M. Weaver, S. Dunn, Piezoelectric and ferroelectric materials and structures for energy harvesting applications, Energy Environ. Sci. 7 (2014) 25.
[30] H. Yu, T. Huang, M. Lu, M. Mao, Q. Zhang, H. Wang, Enhanced power output of an electrospun PVDF/MWCNTs-based nanogenerator by tuning its conductivity, Nanotechnology 24 (2013), 405401.
[31] Z.H. Liu, C.T. Pan, L.W. Lin, J.C. Huang, Z.Y. Ou, Direct-write PVDF nonwoven fiber fabric energy harvesters via the hollow cylindrical near-field electrospinning process, Smart Mater. Struct. 23 (2014) 25003.
[32] N.R. Alluri, B. Saravanakumar, S.J. Kim, Flexible, hybrid piezoelectric film $(BaTi_{(1-x)}Zr_xO_3)$/PVDF nanogenerator as a self-powered fluid velocity sensor, ACS Appl. Mater. Interfaces 7 (2015) 9831–9840.
[33] Z.Y. Jiang, G.P. Zheng, K. Zhan, Z. Han, J.H. Yang, Formation of piezoelectric β-phase crystallites in poly(vinylidene fluoride)-graphene oxide nanocomposites under uniaxial tensions, J. Phys. D Appl. Phys. 48 (2015) 245303.
[34] K.Y. Lee, B. Kumar, J.S. Seo, K.H. Kim, J.I. Sohn, S.N. Cha, D. Choi, Z.L. Wang, S.W. Kim, P-type polymer-hybridized high-performance piezoelectric nanogenerators, Nano Lett. 12 (2012) 1959–1964.
[35] S.Y. Chung, S. Kim, J.H. Lee, K. Kim, S.W. Kim, C.Y. Kang, S.J. Yoon, Y.S. Kim, All-solution-processed flexible thin film piezoelectric nanogenerator, Adv. Mater. 24 (2012) 6022–6027.
[36] K.Y. Lee, J. Bae, S. Kim, J.H. Lee, G.C. Yoon, M.K. Gupta, S. Kim, H. Kim, J. Park, S.W. Kim, Depletion width engineering via surface modification for high performance semiconducting piezoelectric nanogenerators, Nano Energy 8 (2014) 165–173.
[37] L. Zhai, S.I. Khondaker, J. Thomas, C. Shen, M. McInnis, Ordered conjugated polymer nano- and microstructures: structure control for improved performance of organic electronics, Nano Today 9 (2014) 705–721.
[38] R. Rieger, D. Beckmann, A. Mavrinskiy, M. Kastler, M. Klaus, Backbone curvature in polythiophenes, Chem. Mater. 22 (2010) 5314–5318.
[39] M.H. Choi, K.W. Song, D.K. Moon, J.R. Haw, Effect of side chains on solubility and morphology of poly(benzodithiohene-alt-alkylbithiophene) in organic photovoltaics, J. Ind. Eng. Chem. 29 (2015) 120–128.
[40] G. Malliaras, J. Salem, P. Brock, C. Scott, Electrical characteristics and efficiency of single-layer organic light-emitting diodes, Phys. Rev. B 58 (1998) R13411–R13414.
[41] J.-H. Lee, K.Y. Lee, B. Kumar, N.T. Tien, N.-E. Lee, S.-W. Kim, Highly sensitive stretchable transparent piezoelectric nanogenerators, Energy Environ. Sci. 6 (2013) 169–175.
[42] J.H. Lee, K.Y. Lee, M.K. Gupta, T.Y. Kim, D.Y. Lee, J. Oh, C. Ryu, W.J. Yoo, C.Y. Kang, S.J. Yoon, J.B. Yoo, S.W. Kim, Highly stretchable piezoelectric-pyroelectric hybrid nanogenerator, Adv. Mater. 26 (2014) 765–769.
[43] H. Roshani, S. Dessouky, A. Montoya, A.T. Papagiannakis, Energy harvesting from asphalt pavement roadways vehicle-induced stresses: a feasibility study, Appl. Energy 182 (2016) 210–218.
[44] D.H. Lee, J. Shin, M.J. Cho, D.H. Choi, High-performance low-bandgap conjugated polymers bearing diethynylanthracene units for thin-film transistors, Chem. Commun. 49 (2013) 3896.
[45] S. Chen, J.R. Manders, S. Tsang, F. So, Metal oxides for interface engineering in polymer solar cells, J. Mater. Chem. 22 (2012) 24202–24212.

Biographies

Eui Jin Ko received his B.S. degree from the Department of Materials Chemistry and Engineering, Konkuk University, Korea in 2012. He is currently a Ph.D. candidate in the Nano & Information Materials Laboratory, Department of Materials Chemistry and Engineering, Konkuk University, Korea under Prof. Doo Kyung Moon's supervision. His research interests are in conducting polymers and piezoelectric nanogenerators.

Eui Jin Lee received his B.S. degree from the Department of Materials Chemistry and Engineering, Konkuk University, Korea in 2011. He is currently a Ph.D. candidate in the Nano & Information Materials Laboratory, Department of Materials Chemistry and Engineering, Konkuk University, Korea under Prof. Doo Kyung Moon's supervision. His research interests focuses on the fabrication, modification and development of organic electronic devices.

Min Hee Choi is a postdoctoral researcher in the Nano & Information Materials Laboratory, the Department of Materials Chemistry and Engineering, Konkuk University, Korea. She received her B.S. degree in 2009, her M.S. degree in 2011 and her Ph.D. degree in 2016, all from the Department of Materials Chemistry and Engineering, Konkuk University, Korea. Her research interests are in polymer solar cells and organic semiconductors.

Tae Hyun Sung received a B.A. (1982), an M.S. (1987) in inorganic material engineering from Hanyang University and a Ph.D. (1991) in Material Science and Engineering from Tokyo Institute of Technology. He worked at International Superconductivity Technology Center (ISTEC) as a researcher (1992). He was in Massachusetts Institute of Technology (MIT) as a Post doc. (1995). He worked at the Korea Electric Power Research Institute (KEPRI) as a group leader of superconductivity group. Also, he was selected as a "Top 100 Engineers" by IBC (International Biographic Centre), is the member of the National Academy of Engineering of Korea (NAEK). Since 2009, he has been professor of Department of Electrical Engineering, Hanyang University. His research interests include superconductivity, electrical material, energy storage device, and piezoelectric energy harvesting technology.

Doo Kyung Moon received his Ph.D. from Tokyo Institute of Technology, Japan in 1993, and had post-doc experience at the University Arizona in USA (1993–1994) and the Korea Institute of Science and Technology (KIST, 1994–1995). Now, he is a professor of the Department of Materials Chemistry and Engineering, Konkuk University, Korea. He was an adjunct professor of Advanced Industrial Science and Technology (AIST, 2009–2010). His research group works on the development of organic materials and organic electronic devices for organic solar cells, organic light emitting diodes and piezoelectric nanogenerators. For details please see the lab website: http://nanoscience.or.kr